Reducing Climatic Bias in SDG 15.3.1 Land Degradation Assessments Using a Hybrid Productivity Approach: A Remote Sensing Analysis for Northern and Central Morocco (2000–2022)

Nikhil Raghuvanshi *, Nima Ahmadian, Olena Dubovyk

Posted Date: 3 March 2026

doi: 10.20944/preprints202603.0221.v1

Keywords: land degradation neutrality; SDG 15.3.1; Google Earth Engine; hybrid productivity indicator; rain use efficiency; RESTREND; dryland monitoring

 doi:10.20944/preprints202603.0221.v1

Article

Reducing Climatic Bias in SDG 15.3.1 Land Degradation Assessments Using a Hybrid Productivity Approach: A Remote Sensing Analysis for Northern and Central Morocco (2000–2022)

Nikhil Raghuvanshi *, Nima Ahmadian, Olena Dubovyk

Institute of Geography, University of Hamburg, 20146 Hamburg, Germany
* Correspondence: nikhil.raghuvanshi@uni-hamburg.de

Abstract

Land degradation assessments for SDG 15.3.1 often misinterpret rainfall-driven vegetation fluctuations as human-induced decline, particularly in dryland environments where vegetation productivity responds strongly to precipitation variability. This study addresses this challenge by presenting a national-scale land degradation assessment (2000–2022) using a fully reproducible Google Earth Engine workflow that integrates 30 m Landsat time-series NDVI, precipitation, land cover, and soil organic carbon datasets. The core contribution is a precipitation-conditioned hybrid productivity indicator that adaptively selects among NDVI trends, Rain Use Efficiency (RUE), and Residual Trends (RESTREND) according to local precipitation dynamics. This framework operationalizes a climate-aware implementation of the land productivity (LP) sub-indicator within SDG 15.3.1 and enables systematic comparison among productivity metrics under varying rainfall conditions. Results for the 2015–2022 monitoring period, which included multiple drought years, indicate that 18% of land showed declining productivity, 75% remained stable, and 6% showed improvement. Decline was spatially concentrated in arid and semi-arid regions, whereas irrigated and managed landscapes exhibited localized improvements. The hybrid indicator provides an additional option for LP assessment that explicitly accounts for precipitation variability, supporting more climate-sensitive interpretation of productivity trends. This transferable, reproducible methodology strengthens national capacity for SDG 15.3.1 reporting and offers a scalable framework for land degradation assessments in other drought-prone regions.

Keywords: land degradation neutrality; SDG 15.3.1; Google Earth Engine; hybrid productivity indicator; rain use efficiency; RESTREND; dryland monitoring

1. Introduction

Land degradation (LD) is defined by the United Nations Convention to Combat Desertification (UNCCD) as the reduction or loss of the biological or economic productivity and complexity of rainfed cropland, irrigated cropland, or range, pasture, forest, and woodlands resulting from land use or from a combination of processes [1]. It affects approximately 3.2 billion people globally and poses serious risks to food security, ecosystem stability, and sustainable development [2]. The economic consequences are substantial, with global annual losses in productivity and ecosystem services estimated to range between USD 6.3 and 10.6 trillion [3]. If current trends persist, nearly 95% of the Earth's land could become degraded by 2050 [4].

Northern and central Morocco are particularly vulnerable to land degradation due to their Mediterranean to semi-arid climatic conditions and strong interannual rainfall variability. These environments are characterized by pronounced precipitation gradients, elevation contrasts, and widespread dependence on rain-fed agriculture and rangelands. The primary drivers of land degradation in this region

 doi:10.20944/preprints202603.0221.v1

include overgrazing, deforestation, unsustainable farming practices, soil erosion, and salinization [5]. These pressures have reduced soil fertility and vegetation cover in affected areas, posing risks to agricultural productivity, water resources, and rural livelihoods.

Monitoring land degradation consistently across space and time is essential for evaluating its extent and guiding restoration strategies. Sustainable Development Goal (SDG) indicator 15.3.1 was established to measure the proportion of degraded land relative to the total land area [6]. It is the main indicator used to assess progress toward achieving Land Degradation Neutrality (LDN). This composite indicator combines three sub-indicators: land productivity, land cover and land cover change, and carbon stocks [6]. While tools such as `Trends.Earth` have been used to compute this indicator, they are limited by data resolution and processing flexibility [7]. There is a growing need for robust, high-resolution monitoring systems that can be adapted to regional climatic contexts.

Remote sensing, particularly through Earth observation satellites, has become essential for monitoring land degradation under SDG indicator 15.3.1 [8]. These technologies offer broad spatial and temporal coverage, consistent historical data, and cost-effective implementation, making them suitable for assessing degradation and desertification [9]. Platforms such as Google Earth Engine (GEE) and `Trends.Earth` have facilitated access to satellite data and simplified the computation of land degradation indicators [10,11]. While `Trends.Earth` has been widely used in global, regional, and national assessments [11,12], it primarily relies on coarse-resolution datasets and is based on the initial version of the Good Practice Guidance (GPG) provided by the UNCCD [13]. This can lead to reduced accuracy in capturing localized land degradation dynamics [14].

As monitoring needs become more complex and region-specific, there is an increasing demand for flexible, high-resolution, and transparent methods that align with the latest GPG Version 2.0 [15]. Google Earth Engine provides such a platform, supporting scalable analyses using customizable methodologies tailored to regional environmental gradients [16]. Recent studies have demonstrated the advantages of using GEE to produce fine-scale land degradation assessments, with spatial resolutions as high as 30 m, enabling more precise tracking of productivity trends and degradation hotspots [17].

Despite the growing adoption of the SDG 15.3.1 framework, significant methodological uncertainties remain, particularly in measuring land productivity (LP). The most widely used metric for evaluating LP trends is the Normalized Difference Vegetation Index (NDVI), primarily due to its accessibility and long temporal coverage. However, NDVI is sensitive to background noise from soil brightness, atmospheric conditions, and phenological variability [18,19], and can misrepresent true productivity changes, especially in areas experiencing climatic fluctuations rather than land-use-induced degradation [20,21]. This limitation is particularly relevant in Mediterranean to semi-arid environments, where productivity is strongly conditioned by rainfall variability.

Therefore, alternative or complementary indicators are required to better isolate human-induced degradation from climatic variability. Two such alternatives are Rain-Use Efficiency (RUE) [22] and Residual Trends (RESTREND) [23]. However, neither RUE nor RESTREND has been adaptively used within a decision framework conditioned on rainfall dynamics, and no existing SDG 15.3.1 assessments in northern and central Morocco have integrated NDVI, RUE, and RESTREND into a precipitation-conditioned hybrid indicator capable of reducing climate-driven false degradation signals.

This study maps land degradation in northern and central Morocco from 2000 to 2022 using the full SDG indicator 15.3.1 framework, combining land productivity, land cover and land cover change, and carbon stocks. Previous research in Morocco has mostly focused on localized areas, such as land productivity trends in the Souss Massa region [24]. Thus, this study operationalizes a precipitation-adaptive hybrid productivity indicator for regional SDG 15.3.1 assessment by integrating NDVI, RUE, and RESTREND within an author-implemented decision framework conditioned on precipitation (P) dynamics.

Our study addresses the following research questions:

 doi:10.20944/preprints202603.0221.v1

1. How does land degradation evolve within northern and central Morocco between 2000 and 2022 when assessed using the full SDG 15.3.1 indicator framework?
2. How do different land productivity metrics (NDVI, RUE, and RESTREND) compare in detecting land degradation trends across Mediterranean to semi-arid environments?
3. Can combining NDVI, RUE, and RESTREND improve the accuracy and reliability of land productivity assessment within the SDG 15.3.1 framework under precipitation-conditioned dynamics?

2. Materials and Methods

2.1. Study Area

The study area comprises of 9 administrative units located in northern, western, and central Morocco. This region occupies the northwest portion of the country and is bordered by the Mediterranean Sea to the north and the Atlantic Ocean to the west. The landscape includes coastal plains, the Rif Mountains, the Middle and High Atlas mountain systems, inland plateaus, and intensively cultivated agricultural zones.

The region spans Mediterranean, sub-humid, and semi-arid climatic zones, characterized by pronounced spatial and temporal variability in precipitation [25]. Annual rainfall exceeds 1000 mm in parts of the Rif Mountains and decreases progressively toward the inland plateaus and semi-arid transitional zones. Humid areas receiving more than 700 mm of rainfall per year represent a limited proportion of the study area, while sub-humid and semi-arid regions constitute the dominant climatic setting [26]. This strong west–east and elevation-driven rainfall gradient, combined with high interannual variability, provides an appropriate setting for evaluating precipitation-sensitive land degradation indicators.

The climatic and ecological heterogeneity of northern and central Morocco gives rise to diverse agroecological systems, including rain-fed agriculture, irrigated croplands, rangelands, and forested mountain landscapes. Recurrent droughts, erratic rainfall, deforestation, overgrazing, and unsustainable agricultural practices represent key drivers of land degradation within this region [5,27]. Areas dependent on rain-fed agriculture and pastoral systems are particularly sensitive to climatic variability, where declines in land productivity and soil quality have been reported over recent decades.

These strong spatial and temporal climatic contrasts challenge NDVI-only productivity assessments and highlight the importance of indicators that explicitly account for precipitation variability. Given the heterogeneity of Mediterranean to semi-arid environments within northern and central Morocco, regional responses to drought, land use change, and rainfall anomalies vary substantially, reinforcing the need for a spatially adaptive productivity assessment approach tailored to this climatic gradient.

 doi:10.20944/preprints202603.0221.v1

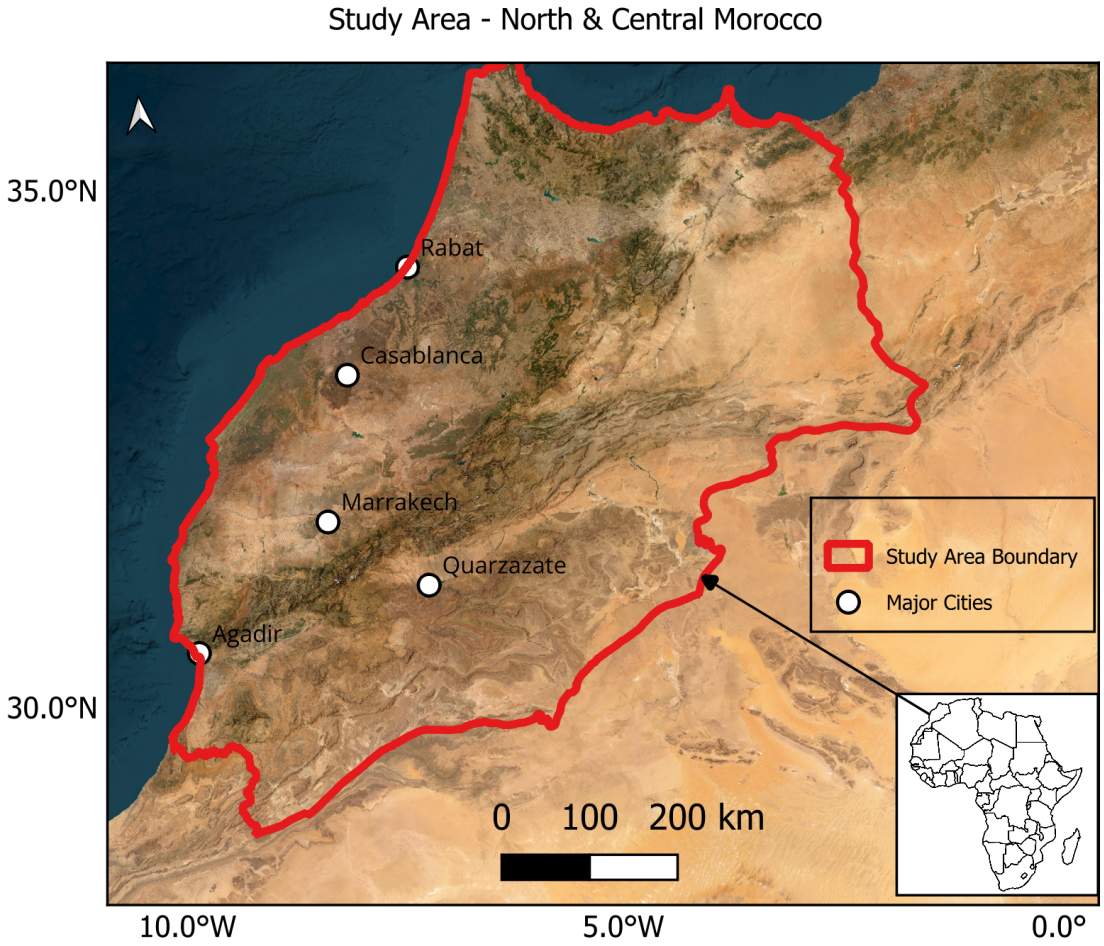

Figure 1. Location and geographical context of the study area of North and Central Morocco and the position of Morocco within the African continent.

2.2. Datasets

This study assesses land degradation in accordance with the SDG Indicator 15.3.1 framework using its three sub-indicators: Land Cover (LC), Land Productivity (LP), and Soil Organic Carbon (SOC). Landsat Collection 2 Level-2 Surface Reflectance data were corrected using standard surface reflectance scaling factors and cloud- and shadow-masked using `QA_PIXEL` bitmasks. Annual NDVI, Rain Use Efficiency (RUE), and Residual Trend (RESTREND) metrics were computed using annual composites.

For LP, the analysis extends beyond NDVI by incorporating RUE and RESTREND methods to explicitly account for the influence of precipitation variability. Rainfall data were sourced from the Climate Hazards Group InfraRed Precipitation with Stations (CHIRPS) dataset. Monthly and daily CHIRPS precipitation data were aggregated to annual totals for LP modeling and precipitation trend estimation. Although SOC data are available at a spatial resolution of 250 m, soil carbon stocks change gradually at the landscape scale, making the dataset suitable for integration with 30 m LC and LP layers at national extent.

The datasets, spatial resolutions, temporal coverage, and references used in this study are summarized in Table 1. All dataset selection and preprocessing followed the UNCCD Good Practice Guidance Version 2.0 for SDG 15.3.1 reporting.

 doi:10.20944/preprints202603.0221.v1

Table 1. Summary of land degradation (LD) sub-indicators used for the SDG 15.3.1 assessment, including their conceptual description, spatial resolution, temporal coverage, and corresponding data sources.

LD Sub-Indicator	Description	Spatial Resolution	Temporal Coverage	Data Source
Land Cover (LC)	Land cover classification to track land-use changes and transitions over time.	30 m	2000, 2015, 2022	GLC_FCS30D [28]
Land Productivity (LP)	Productivity trends derived from NDVI, Rain Use Efficiency (RUE), and Residual Trend (RESTREND) using optical satellite data and precipitation.	30 m; 0.05°	2000–2022	Landsat 5/7/8 [29], CHIRPS [30]
Soil Organic Carbon (SOC)	Soil organic carbon stock estimates derived from machine-learning-based global models.	250 m	2000, 2015, 2022	OpenLandMap SOC [31]

2.3. Methodology

2.3.1. Land Cover and Land Cover Change

Land cover transitions are a fundamental sub-indicator of the UNCCD Sustainable Development Goal (SDG) 15.3.1 framework because they record whether a land unit maintains its ecological function or shifts toward a less productive state. To maximize interpretability and reproducibility, the land cover workflow was redesigned from first principles using high-resolution data, a clear class hierarchy, and open-source processing. National-scale land cover maps were derived from the GLC_FCS30D dataset (version 2023), which provides annual land cover classifications at 30 m spatial resolution based on multi-sensor Landsat and Sentinel imagery. All processing was conducted in Google Earth Engine (GEE).

The original 23 land cover classes were reclassified into seven UNCCD-compliant categories: cropland, forest, grassland, wetland, artificial surfaces, bare land, and water, following the UNCCD Good Practice Guidance (GPG) Version 2.0. Land cover maps were generated for the beginning of the baseline period (2000), the midpoint (2015), and the end of the monitoring period (2022).

Land cover change was quantified by constructing transition matrices for the baseline (2000–2015) and monitoring (2015–2022) periods. Each transition was assigned one of three states using a rule-based ecological hierarchy. Transitions from higher to lower ecosystem service provision (e.g., forest to cropland or grassland to artificial surfaces) were classified as *declining*. Transitions with no ecologically meaningful change were classified as *stable*, while transitions from lower to higher productivity (e.g., cropland to forest or artificial surfaces to wetland) were classified as *improving*. These rules follow the UNCCD GPG 2.0 and are detailed in Appendix A.

By differentiating ecologically meaningful gains and losses rather than treating all changes as degradation, this approach distinguishes restoration dynamics from anthropogenic pressure. To visualize land cover transitions, and land cover degradation maps were produced for the study areas and complete transition matrices are provided in the Appendix, while only key figures and trends are summarized in the main text.

2.3.2. Soil Organic Carbon

Soil organic carbon (SOC) stocks serve as an integrative indicator of land condition and ecosystem integrity. While comprehensive carbon stock assessments ideally include biomass from woody vegetation, grasslands, croplands, and root systems, such data are often sparse and inconsistent at national and regional levels [32]. As a result, soil organic carbon (SOC), which represents the largest share of terrestrial carbon, is frequently used as a proxy for tracking degradation trends [33]. SOC change was estimated using a Tier 1 stock-change factor approach, in which a reference SOC layer is multiplied by land-use conversion coefficients derived from land cover transitions. A reference SOC map derived from the Harmonized World Soil Database was paired with a land-use coefficient matrix to estimate carbon gains or losses for each transition.

 doi:10.20944/preprints202603.0221.v1

Recognizing that Tier 1 coefficients [34] represent global averages and may not fully capture Moroccan conditions, a region-specific correction factor of 0.48 was applied for transitions involving cropland, following IPCC guidance for tropical moist environments. SOC for each pixel and period was calculated as:

$$SOC_{\text{final}} = SOC_{\text{ref}} \times c_{\text{lu}}, \tag{1}$$

where c_{lu} is the land-use coefficient associated with the observed land cover transition.

SOC was computed for both the baseline period (2000–2015) and the monitoring period (2015–2022), and the percentage change in SOC was calculated as:

$$\Delta SOC(\%) = \frac{SOC_{\text{final}} - SOC_{\text{ref}}}{SOC_{\text{ref}}} \times 100. \tag{2}$$

SOC changes were classified into three categories: *declining* for losses exceeding 10%, *stable* for changes within ±10%, and *improving* for gains greater than 10%. Limiting classification to three categories avoids spurious precision and aligns with UNCCD GPG 2.0 recommendations. Detailed coefficients and example calculations are provided in the Supplementary Tables. Uncertainty associated with Tier 1 SOC estimates, particularly their limited sensitivity to management practices and local soil properties, is addressed in the Discussion.

2.3.3. Land Productivity

Land productivity reflects the capacity of vegetation to convert sunlight, water, and nutrients into biomass. While Net Primary Productivity (NPP) is a direct measure of this process, its estimation is resource-intensive and rarely feasible across large spatial and temporal scales. As an alternative, the Normalized Difference Vegetation Index (NDVI) is widely used due to its established correlation with photosynthetic activity and vegetation dynamics [35,36]. Numerous studies have demonstrated the effectiveness of NDVI as Mean growing-season NDVI and annual average NDVI in capturing both seasonal and long-term changes in vegetation and its value as a proxy for assessing land degradation trends [19,37,38]. According to the SDG Indicator framework, land productivity was assessed using a three-component framework consisting of trend, state, and performance.

The trend component captured the long-term direction of productivity change using pixel-wise regression analysis of NDVI, Rain Use Efficiency (RUE), and Residual Trends (RESTREND). A significant negative trend in NDVI, RUE, or RESTREND residuals indicated declining productivity, while a significant positive trend indicated improvement. Non-significant trends were classified as stable. NDVI trends were derived at the pixel level using linear regression and the Mann Kendall significance test [39,40]

Rain Use Efficiency (RUE) [22] was used to normalize vegetation productivity by rainfall and was calculated as:

$$RUE_t = \frac{NDVI_t}{\sum P_t}, \tag{3}$$

where $NDVI_t$ is the mean annual NDVI for year t, and $\sum P_t$ is cumulative annual precipitation derived from the CHIRPS dataset. RUE reduces the direct influence of interannual rainfall variability and is particularly useful in water-limited environments.

Residual trend analysis (RESTREND) [41] was applied to isolate the climate-independent component of NDVI dynamics by modeling NDVI as a linear function of precipitation:

$$NDVI_t = \alpha + \beta P_t + \epsilon_t, \tag{4}$$

where α is the intercept, β represents precipitation sensitivity, and ϵ_t is the climate-independent residual. Temporal trends in ϵ_t were used to identify non-climatic productivity change.

The state component assessed whether recent productivity deviated from long-term conditions. For each pixel, annual mean NDVI values were aggregated into a long-term reference period and a recent period. For the baseline assessment, 2000–2011 served as the reference period and 2012–2014 as

 doi:10.20944/preprints202603.0221.v1

the recent window. For the monitoring assessment, 2015–2019 was used as the reference period and 2020–2022 as the recent window. A standardized Z-score was calculated as:

$$Z = \frac{\overline{NDVI}_{\text{recent}} - \mu_{\text{long}}}{\sigma_{\text{long}} / \sqrt{n}}, \tag{5}$$

where μ_{long} and σ_{long} are the pixel-wise mean and standard deviation of NDVI during the reference period, and $n = 3$ years is the length of the recent window. Pixels were classified as declining if $Z < -1.96$, improving if $Z > 1.96$, and stable otherwise. The Land Productivity (LP) performance sub-indicator evaluates local vegetation vigor relative to ecologically similar regions defined by the intersection of OpenLandMap SOC soil taxonomy groups and land cover (LC) classes as detailed in Table 1 [42]. To establish a benchmark for maximum potential productivity, the 90th percentile of NDVI was calculated for each unique ecoregion ($NDVI_{max}$). The LP performance for each pixel is then determined by calculating the ratio between the observed mean NDVI and the corresponding $NDVI_{max}$ value. Consistent with established methodologies [43], performance values below 0.5 represent areas where productivity was significantly lower than their ecological potential, indicating that land degradation may be prevalent. The trend, state and performance component are combined together using the GPG Version 2 guidelines and the decision table can be obtained in Appendix B.

2.4. Hybrid Component (Precipitation-Conditioned Land Productivity Indicator)

To reduce climate-driven misclassification in Mediterranean to semi-arid environments, we developed a precipitation-conditioned hybrid land productivity indicator that adaptively selects the most appropriate productivity metric based on local rainfall dynamics. The conceptual logic of this approach is illustrated in Figure 2.

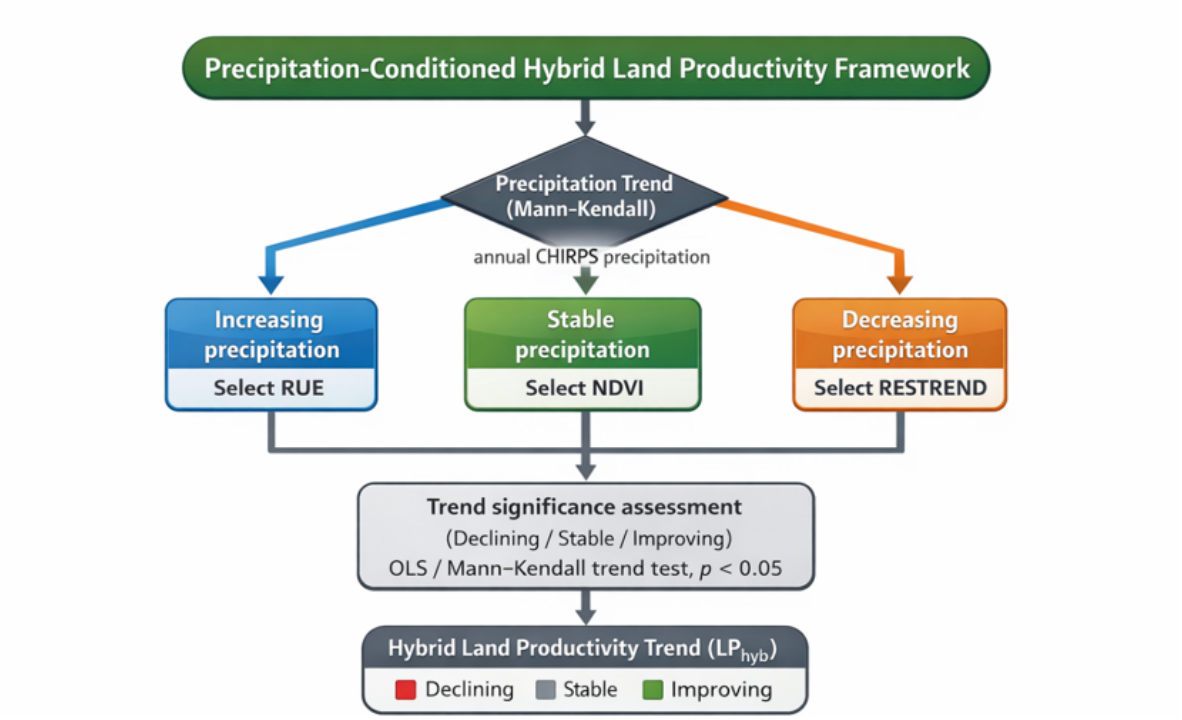

Figure 2. Conceptual precipitation-conditioned hybrid land productivity framework. When precipitation trends are increasing, the Rain Use Efficiency (RUE) index is applied to normalize vegetation greenness by rainfall. Under stable precipitation conditions, NDVI is used as climatic noise is minimal. Under decreasing precipitation, RESTREND residuals are employed to detect management-driven resilience or decline.

Vegetation productivity in drylands is strongly constrained by precipitation variability. When rainfall increases, NDVI may show greening trends that reflect climatic improvement rather than land management. Conversely, under drying conditions, NDVI declines may simply reflect reduced

 doi:10.20944/preprints202603.0221.v1

rainfall rather than anthropogenic degradation. Therefore, using a single productivity metric across heterogeneous precipitation regimes can lead to misclassification of degradation signals.

To address this limitation, we implemented a rule-based switching framework conditioned on pixel-wise precipitation trends. First, annual CHIRPS precipitation totals were analyzed using the non-parametric Mann–Kendall trend test. Each pixel was classified into one of three precipitation trend categories: significantly increasing, stable (non-significant), or significantly decreasing.

The hybrid logic follows three decision rules:

- Under significantly increasing precipitation, Rain Use Efficiency (RUE) is applied to normalize vegetation greenness by rainfall and suppress rainfall-driven greening signals.
- Under stable precipitation conditions, NDVI is retained as a direct proxy for vegetation activity since climatic noise is minimal.
- Under significantly decreasing precipitation, RESTREND residuals are used to isolate climate-independent productivity changes and detect management-driven resilience or decline.

This conceptual switching framework is formalized as:

$$LP_{\text{hyb}}(x) = \begin{cases} LP_{\text{RUE}}(x), & \text{if } T_P(x) = +1, \\ LP_{\text{NDVI}}(x), & \text{if } T_P(x) = 0, \\ LP_{\text{RESTREND}}(x), & \text{if } T_P(x) = -1, \end{cases} \tag{6}$$

where $T_P(x)$ denotes the precipitation trend class at pixel x.

The resulting hybrid productivity trend map was classified into declining, stable, and improving categories using the same statistical significance criteria applied to the selected underlying metric. This precipitation-conditioned switching scheme provides a transparent, reproducible, and policy-aligned framework to reduce rainfall-induced confounding while maintaining interpretability for SDG Indicator 15.3.1 reporting.

2.5. Integration into SDG Indicator 15.3.1

To derive the overall SDG 15.3.1 land-degradation indicator, the three sub-indicators (i.e., land cover change, soil organic carbon (SOC) change, and the land productivity indicator) were integrated using a rule-based majority approach following the UNCCD Good Practice Guidance (GPG v2.0) as sgown in Figure 3. For each assessment period (baseline: 2000–2015; monitoring: 2015–2022), pixels were classified as degraded if at least two sub-indicators indicated decline, improved if at least two indicated improvement, and stable otherwise. To derive a binary degradation map emphasizing areas of emerging risk, a precautionary criterion (hereafter referred to as Rule B) was applied across periods. Under this rule, a pixel was classified as degraded if it was degraded in the monitoring period or if its status worsened relative to the baseline period. Pixels that remained stable or improved were classified as non-degraded. Only pixels with valid data across all three sub-indicators in both periods were retained in the final analysis. Detailed rule matrices and logical combinations are provided in Appendix C.

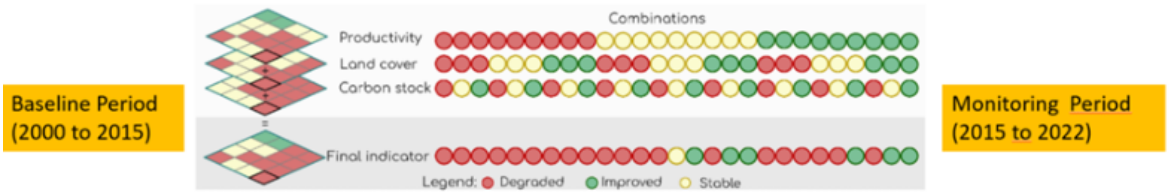

Figure 3. Conceptual illustration of the integration of land productivity, land cover, and soil organic carbon sub-indicators to derive the final SDG 15.3.1 land-degradation indicator for the baseline (2000–2015) and monitoring (2015–2022) periods.

 doi:10.20944/preprints202603.0221.v1

3. Results

3.1. Land Cover and Land Cover Change

3.1.1. Land Cover Patterns

The reclassified land-cover maps indicate that the study area is dominated by the *other land* class, comprising bare areas, rocky terrain, desert surfaces, and sparsely vegetated rangelands (Figure 4). This class covered approximately 34.7 Mha in 2000 and remained largely stable throughout the study period. Forests occupied roughly 10 Mha, primarily distributed along the Atlas and Rif mountain ranges and in the northern coastal region. Cropland was concentrated in the northern and central plains, while grassland and wetland classes occurred in spatially fragmented patterns. Artificial surfaces represented a small but gradually increasing fraction of national land cover ($< 0.7\%$), mainly surrounding major urban centers.

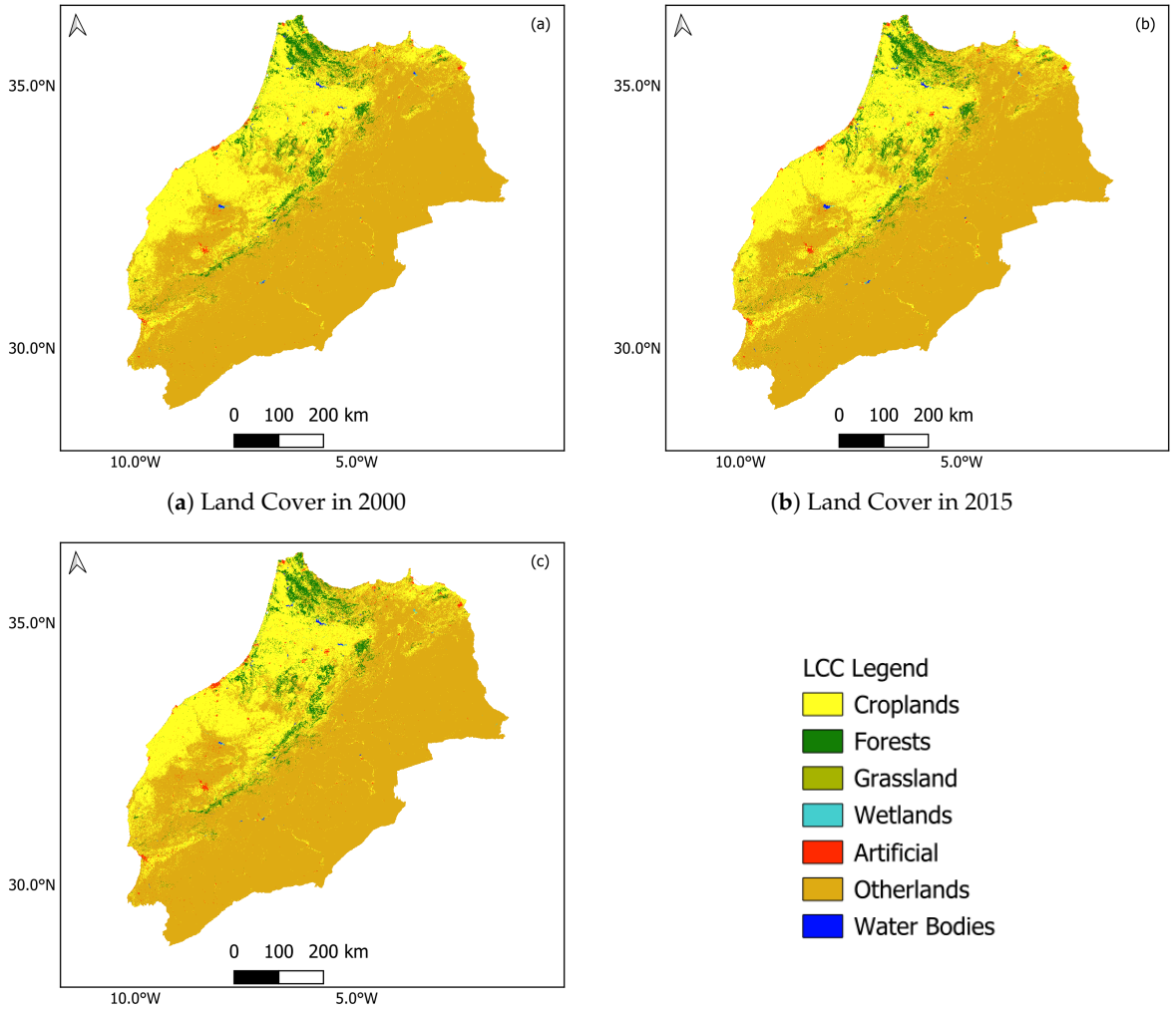

(**a**) Land Cover in 2000

(**b**) Land Cover in 2015

(**c**) Land Cover in 2022

(**d**) LC Legend

Figure 4. Spatiotemporal patterns of national land cover in Morocco: (a) 2000; (b) 2015; and (c) 2022. The maps are derived from reclassified GLC_FCS30D data at 30 m resolution. The legend (d) illustrates the six primary reclassified classes used for this study.

3.1.2. Land-Cover Transition Dynamics

Between 2000 and 2015, the majority of the study area remained stable. The most prominent directional transition during the baseline period was the conversion from *other land* to *forest*, amounting to approximately 1.08 Mha, consistent with national reforestation and restoration efforts. At the same

 doi:10.20944/preprints202603.0221.v1

time, forest losses totaling about 0.83 Mha were observed, indicating localized degradation and land conversion.

Table 2 summarizes the main land-cover transitions during each assessment period, while full transition matrices are provided in Appendix D.

Table 2. Major land-cover transitions in the study area during the baseline and monitoring periods.

Period	Key Transition	Area (Mha)	Interpretation
2000–2015	Other land → Forest	1.08	Net increase in forest cover due to afforestation and restoration activities.
2000–2015	Forest → Other land	0.83	Localized forest loss linked to land degradation or forest cover conversion processes.
2015–2022	Other land → Forest	0.60	Continued but reduced forest expansion during the monitoring period.
2015–2022	Forest → Other land	0.87	Persistent pressure on forests despite restoration efforts.

3.1.3. Land Cover Change Classification

Applying the UNCCD land-cover decision rules resulted in 1.36 Mha of degraded land and 1.22 Mha of improved land during the baseline period, yielding a net decline of 0.14 Mha. In the monitoring period, degraded areas remained similar (1.22 Mha), while improved areas decreased to 0.74 Mha, increasing the net loss to 0.48 Mha.

Maps of land-cover degradation, stability, and improvement (Figure 5) show that degradation hotspots are concentrated in peri-urban areas and intensively grazed rangelands, whereas improvements are more widespread in afforested northern mountains and irrigated croplands.

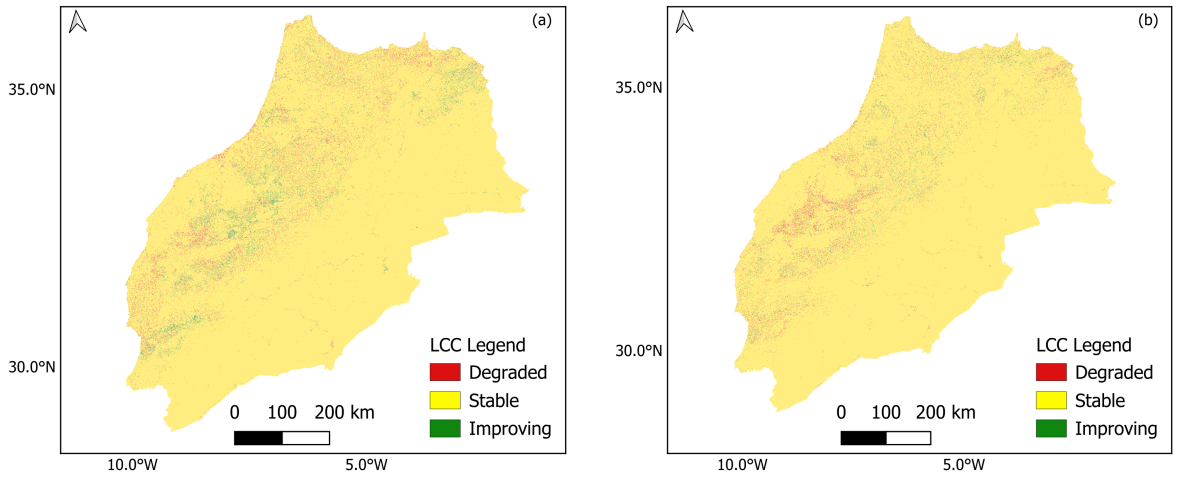

(**a**) LCC (Baseline period, 2000–2015) (**b**) LCC (Monitoring period, 2015–2022)

Figure 5. Spatial distribution of the land cover change degradation patterns for the baseline (2000–2015) and monitoring (2015–2022) periods in the study area.

3.2. Soil Organic Carbon

Across the study area, approximately 0.91 Mha (2.1% of the land area) exhibited soil organic carbon (SOC) losses greater than 10% during 2000–2015 (Table 3). About 1.14 Mha (2.6%) showed SOC gains exceeding 10%, while the remaining 95.3% of land remained stable.

During 2015–2022, the proportion of degraded area decreased is 2.1% of the study area and the share of improving area also declined to 1.5% compared to the baseline period. More than 96.4% of study area's land maintained stable SOC levels during the monitoring period. The reduction in improving areas likely reflects prolonged drought conditions combined with limited soil conservation

 doi:10.20944/preprints202603.0221.v1

investments. Because SOC changes were derived solely from land-cover transitions, fine-scale soil management effects are not captured, highlighting the need for higher-resolution SOC datasets.

Table 3. Soil organic carbon (SOC) status in Morocco for two assessment periods.Area is reported in million hectares (Mha), and share (%) represents the proportion of the total land area of the study area.

SOC Status	Area (2000–2015) (Mha)	Share (%)	Area (2015–2022) (Mha)	Share (%)
Degraded (>10% loss)	0.76	2.1	0.75	2.0
Stable (±10%)	34.62	94.6	35.05	95.6
Improved (>10% gain)	0.95	2.6	0.54	1.5
Total	43.13	100.0	43.13	100.0

Soil Organic Carbon (SOC) status distribution for the baseline (2000–2015) and monitoring (2015–2022) periods.

3.3. Land Productivity

3.3.1. NDVI, RUE, and RESTREND Indicators

The NDVI-based trend analysis indicated a strong apparent improvement during the baseline period (2000–2015), with 35.07 Mha (96.27%) of the study area classified as improving, 1.34 Mha (3.68%) as stable, and only 0.02 Mha (0.05%) as declining (Table 4). In contrast, during the monitoring period (2015–2022), declining NDVI trends increased substantially to 3.96 Mha (10.87%), while stable areas dominated with 30.02 Mha (82.40%), and improving areas decreased sharply to 2.45 Mha (6.73%). This shift highlights the sensitivity of NDVI to interannual rainfall variability and recent drought conditions.

RUE and RESTREND produced more conservative and stable patterns compared to NDVI. During 2000–2015, RUE classified 25.88 Mha (71.04%) as stable, 10.46 Mha (28.71%) as improving, and only 0.09 Mha (0.25%) as declining. Similarly, RESTREND indicated 25.76 Mha (70.27%) stable, 10.74 Mha (29.31%) improving, and 0.15 Mha (0.42%) declining.

In the monitoring period (2015–2022), both RUE and RESTREND showed a strong dominance of stable conditions. RUE classified 33.84 Mha (92.31%) as stable, 2.68 Mha (7.32%) as improving, and only 0.14 Mha (0.37%) as declining. RESTREND results were nearly identical, with 33.99 Mha (92.73%) stable, 2.53 Mha (6.91%) improving, and 0.13 Mha (0.36%) declining.

Table 4. Area and share of land productivity classes (declining, stable, and improving) in the study area for the baseline period (2000–2015) and the monitoring period (2015–2022), derived from NDVI, Rain Use Efficiency (RUE), and Residual Trend (RESTREND) indicators. Area is reported in million hectares (Mha), and share (%) represents the proportion of the total study area.

Period	Indicator	Declining (Mha)	Share (%)	Stable (Mha)	Share (%)	Improving (Mha)	Share (%)
2000–2015	NDVI	0.02	0.05	1.34	3.68	35.07	96.27
	RUE	0.09	0.25	25.88	71.04	10.46	28.71
	RESTREND	0.15	0.42	25.76	70.27	10.74	29.31
2015–2022	NDVI	3.96	10.87	30.02	82.40	2.45	6.73
	RUE	0.14	0.37	33.84	92.31	2.68	7.32
	RESTREND	0.13	0.36	33.99	92.73	2.53	6.91

Spatially, NDVI trends improvements during the baseline period were widespread, particularly in central and southern Morocco. In the monitoring period, degradation hotspots emerged across the northern plains and southwestern margins, corresponding to severe drought episodes between 2016 and 2020. RUE and RESTREND maps exhibited more spatially consistent patterns, with dominant stability across most regions and localized improvements primarily in northern and eastern areas where rainfall variability decreased. Agreement between RUE and RESTREND reached 66.4% in the baseline and 22.1% in the monitoring period. The spatial patterns of land productivity (LP) trends derived from NDVI, Rain Use Efficiency (RUE), and RESTREND for the baseline and monitoring periods are illustrated in Figure 6.

 doi:10.20944/preprints202603.0221.v1

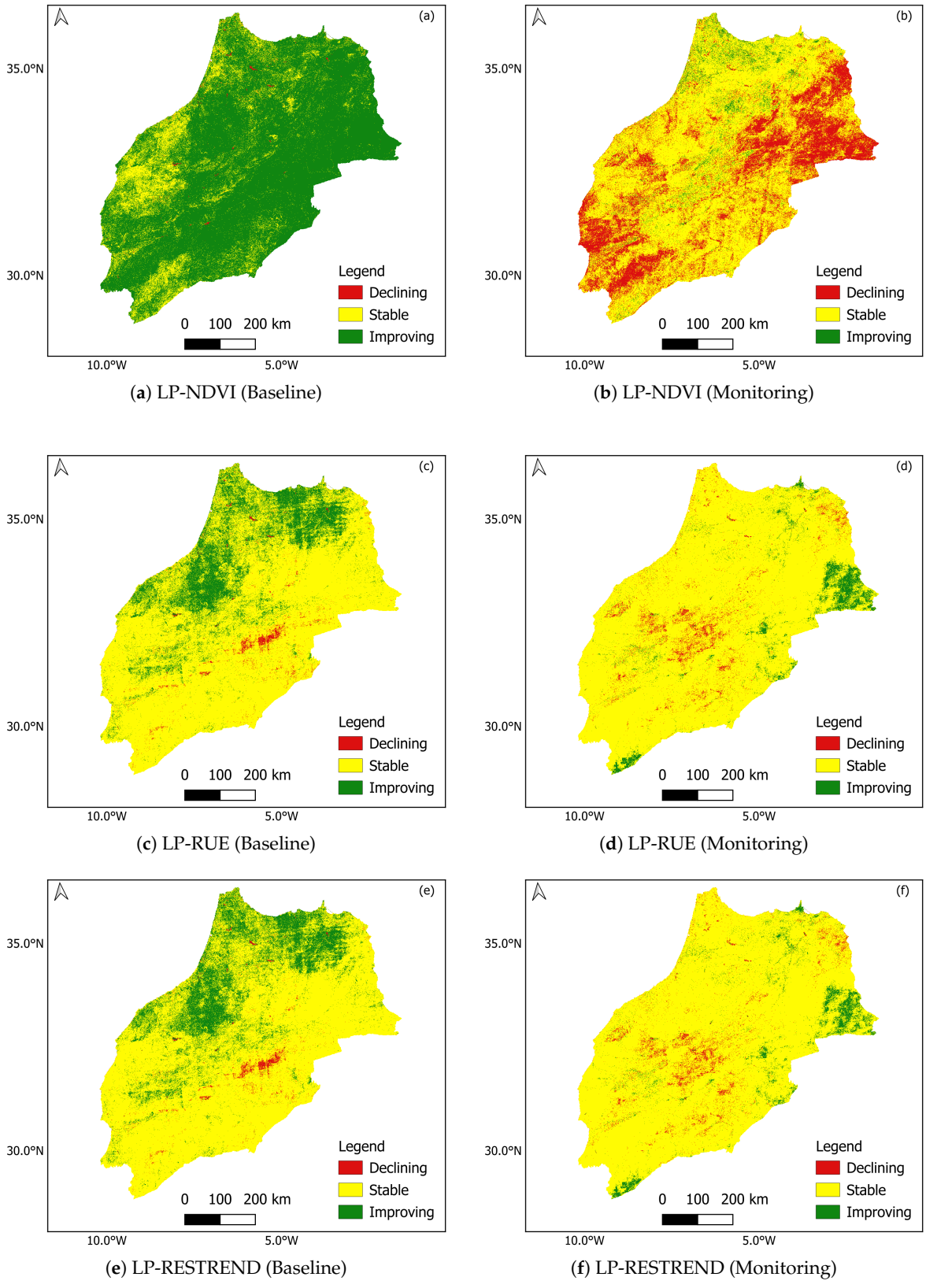

(**a**) LP-NDVI (Baseline) (**b**) LP-NDVI (Monitoring)

(**c**) LP-RUE (Baseline) (**d**) LP-RUE (Monitoring)

(**e**) LP-RESTREND (Baseline) (**f**) LP-RESTREND (Monitoring)

Figure 6. Spatial distribution of LP sub-indicators: (a,b) NDVI; (c,d) RUE; and (e,f) RESTREND for baseline (2000–2015) and monitoring (2015–2022) periods.

 doi:10.20944/preprints202603.0221.v1

3.3.2. Hybrid Productivity Results

The precipitation-conditioned hybrid indicator as described in section 2.4 is shown in Figure 7. During 2000–2015, 45.81% of the study area was classified as improving (16.79 Mha), 51.86% as stable (19.01 Mha), and 1.57% as declining (0.58 Mha).

In 2015–2022, declining areas increased substantially to 18.52% (6.79 Mha), stable areas expanded to 74.93% (27.46 Mha), and improvements declined sharply to 5.80% (2.13 Mha) (Table 5). Compared with NDVI based , the hybrid indicator reduced rainfall-driven improvement signals during wetter years and avoided excessive filtering during drought years.

Table 5. Area and share of the hybrid land productivity indicator classes (declining, stable, and improving) within the study area for the baseline period (2000–2015) and the monitoring period (2015–2022). Area is reported in million hectares (Mha), and share (%) represents the proportion of the total study area excluding masked pixels.

Period	Class	Area (Mha)	Share (%)
2000–2015	Declining	0.58	1.57
	Stable	19.01	51.86
	Improving	16.79	45.81
2015–2022	Declining	6.79	18.52
	Stable	27.46	74.93
	Improving	2.13	5.80

Spatially, the hybrid land productivity indicator reveals clear contrasts between the baseline and monitoring periods (Figure 7). During the baseline period (Figure 7a), improvements dominate large portions of the northern and northwestern parts of the study area, particularly along the Atlantic plains and Rif foothills, reflecting favorable precipitation conditions and stable vegetation response. Central portions are largely classified as stable, with localized degradation hotspots occurring in semi-arid transition zones. In contrast, the monitoring period (Figure 7b) shows a pronounced expansion of degraded areas across central and eastern parts of the study area, coinciding with regions affected by prolonged drought conditions between 2016 and 2020. Improvements become spatially fragmented and are mainly confined to irrigated zones and higher-elevation areas.

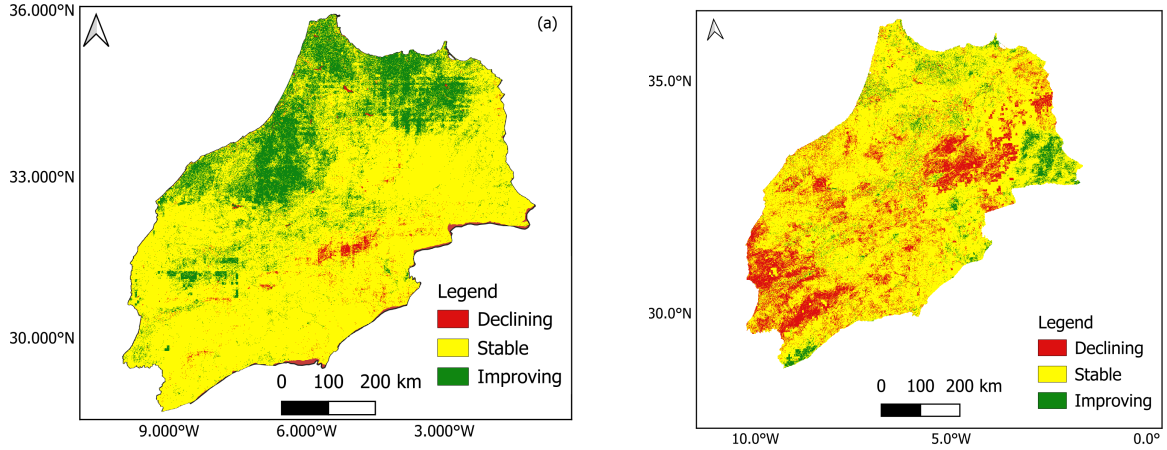

(**a**) Hybrid LP (Baseline period, 2000–2015) (**b**) Hybrid LP (Monitoring period, 2015–2022)

Figure 7. Spatial distribution of the precipitation-conditioned hybrid land productivity indicator for the baseline (2000–2015) and monitoring (2015–2022) periods in Morocco.

3.3.3. Precipitation–Productivity Relationships

Pearson correlation analysis revealed weak positive correlations between NDVI and precipitation, while RUE and RESTREND exhibited negative correlations, reflecting rainfall normalization and

 doi:10.20944/preprints202603.0221.v1

regression-based climate removal (Table 6). Cross-tabulation analyses (Appendix E) showed that under declining precipitation, RUE and RESTREND were better at detecting management-driven productivity changes.

Table 6. Pearson correlation coefficients between precipitation and land productivity indicators (NDVI, RUE, and RESTREND) in the study area for the baseline (2000–2015) and monitoring (2015–2022) periods. All correlations are statistically significant at $p < 0.001$.

Period	Indicator	Correlation (r)
2000–2015	NDVI	0.131
	RUE	−0.426
	RESTREND	−0.423
2015–2022	NDVI	0.232
	RUE	−0.192
	RESTREND	−0.177

3.4. Final SDG 15.3.1 Indicator

The final SDG 15.3.1 binary land degradation (LD) maps were generated by integrating LP, LCC, and SOC using the majority-rule approach combined with the precautionary Rule B. Under Rule B, any sub-indicator signaling degradation classifies the pixel as degraded, thereby providing a conservative estimate and functioning as an early-warning mechanism.

To evaluate the influence of the land productivity metric on final LD outcomes, four LP-based implementations were compared: NDVI-based LP, RUE-based LP, RESTREND-based LP, and the precipitation-conditioned hybrid LP. Each LP variant was independently integrated with the remaining SDG sub-indicators under Rule B to produce four final binary LD maps (Figure 8) and the comparison is shown in Table 7 .

The NDVI-based implementation classified 30.13 Mha as degraded and 6.21 Mha as non-degraded, indicating widespread degradation signals across the study area. In contrast, the RUE-based and RESTREND-based implementations produced substantially lower degradation estimates. The RUE-based map classified 7.86 Mha as degraded and 28.48 Mha as non-degraded, while the RESTREND-based map yielded nearly identical results, with 7.83 Mha degraded and 28.51 Mha non-degraded.

The hybrid-based implementation produced intermediate results, identifying 19.42 Mha as degraded and 17.23 Mha as non-degraded. This represents a balanced outcome between the highly sensitive NDVI-based approach and the more conservative RUE and RESTREND approaches.

Spatially, the NDVI-based LD map (Figure 8a) shows extensive degradation across large portions of the study area, reflecting NDVI's sensitivity to rainfall variability and drought effects. The RUE- and RESTREND-based maps (Figure 8b–c) display more spatially similar degradation patterns, primarily concentrated in semi-arid transition zones and areas of persistent productivity decline. The hybrid-based LD map (Figure 8d) integrates these contrasting signals, reducing rainfall-driven false positives while preserving persistent degradation hotspots.

 doi:10.20944/preprints202603.0221.v1

Table 7. Area and percentage share of degraded and non-degraded land derived from four alternative land productivity (LP) implementations under Rule B within the study area (2000–2022). Area is reported in million hectares (Mha), and percentage share represents the proportion of the total study area.

LP Metric	Class	Area (Mha)	Share (%)
Hybrid	Degraded	19.42	52.99
	Non-degraded	17.23	47.01
NDVI	Degraded	30.13	82.18
	Non-degraded	6.21	17.82
RUE	Degraded	7.86	21.45
	Non-degraded	28.48	78.55
RESTREND	Degraded	7.83	21.36
	Non-degraded	28.51	78.64

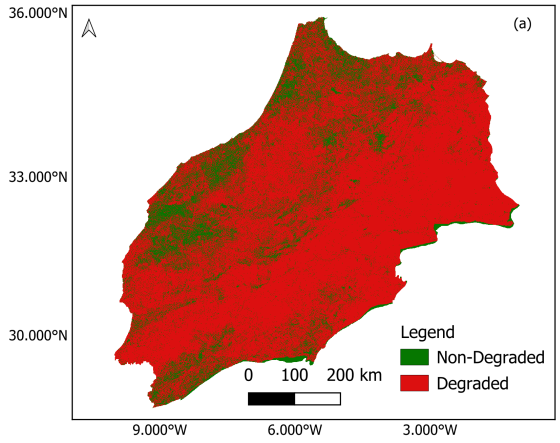

(**a**) Binary LD map based LP-NDVI

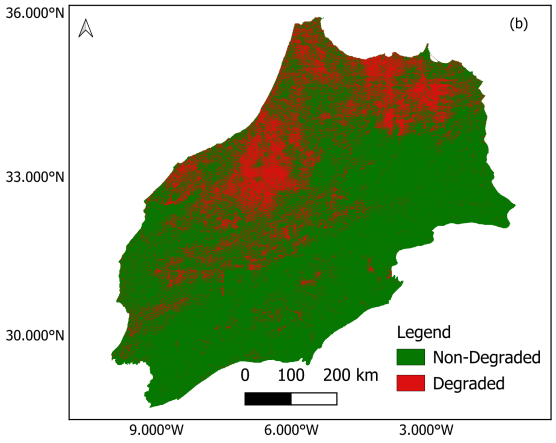

(**b**) Binary LD map based on LP-RUE

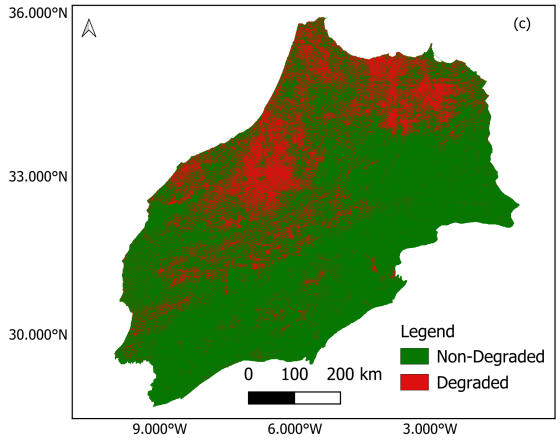

(**c**) Binary LD map basedLP-RESTREND

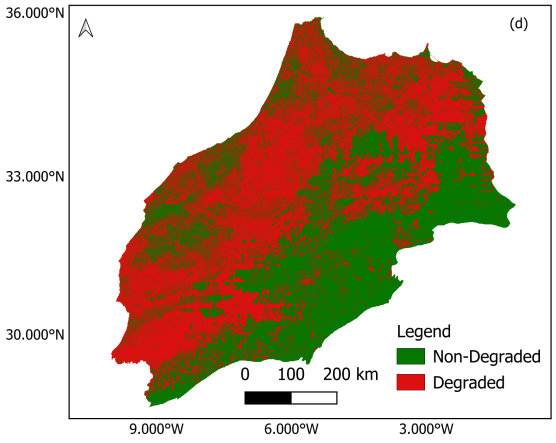

(**d**) Binary LD map based LP-Hybrid

Figure 8. Final SDG 15.3.1 binary land degradation maps derived using Rule B and four alternative land productivity metrics for the period 2000–2022: (a) NDVI-based, (b) RUE-based, (c) RESTREND-based, and (d) precipitation-conditioned hybrid LP.

 doi:10.20944/preprints202603.0221.v1

4. Discussion

4.1. Synthesis of Land-Cover Change and Land Productivity Patterns

The spatio-temporal patterns emerging from the results provide insights beyond numerical summaries. Transition matrices indicate that most of the study area remained in stable land-cover categories across both assessment periods. However, the directional transition from other land to forest decreased from 1.08 Mha during the baseline period (2000–2015) to 0.60 Mha in the monitoring period (2015–2022), signalling a slowdown in afforestation and restoration processes (Table 2). At the same time, forest-to-other land conversion increased slightly from 0.83 Mha to 0.87 Mha, indicating persistent pressure on forest ecosystems. These patterns are consistent with independent assessments reporting continued forest loss of approximately 31,000 ha per year [44].

Application of the UNCCD land-cover decision rules further reveals that degraded land amounted to 1.36 Mha during the baseline period and 1.22 Mha during the monitoring period. However, improved land decreased from 1.22 Mha to 0.74 Mha, increasing the net loss from 0.14 Mha to 0.48 Mha. Although gross degradation remained relatively stable, the reduced area of improvement suggests weakening recovery dynamics in recent years.

Land-cover transitions also highlight nuanced cropland dynamics. Cropland expansion during 2000–2015 was concentrated in northern and central plains, whereas slight declines after 2015 were primarily observed in semi-arid zones. These changes coincided with pronounced drought episodes and reduced viability of rain-fed agriculture. Biodiversity assessments indicate persistent forest loss and increasing water stress in agricultural systems [44], underscoring how climatic pressures and anthropogenic expansion interact to reshape land use.

The land productivity sub-indicator further illustrates how climatic variability influences interpretation of vegetation trends. During the baseline period, the NDVI-based trend classified 96.27% of the territory as improving, while RUE and RESTREND identified improvements on only 28.71% and 29.31% of the area, respectively (Table 4). This stark contrast indicates that NDVI likely overestimated improvement under favourable precipitation conditions. Remote-sensing studies confirm that vegetation in semi-arid environments responds rapidly to rainfall variability [45], and that NDVI is moderately correlated with precipitation [46].

In the drought-affected monitoring period, NDVI classified 10.87% of the area as declining, whereas RUE and RESTREND indicated declines on less than 0.4% of the territory. Meanwhile, more than 92% of the area was classified as stable by rainfall-adjusted indicators. This divergence suggests that precipitation-driven fluctuations strongly influence NDVI trends during dry phases, while rainfall-adjusted metrics filter out short-term climatic variability.

Finally, the spatial agreement among productivity indicators shifted markedly between periods. Agreement between RUE and RESTREND covered roughly two-thirds of the study area during the baseline period, pointing to consistent signals when climatic conditions were favourable. In the monitoring period, agreement across all three indicators rose to more than three-quarters of the country, while RUE-RESTREND agreement declined to about one-fifth. This shift implies that under prolonged drought stress, NDVI becomes more aligned with rainfall-adjusted metrics as water limitations suppress vegetation growth. The convergence of the three indicators under dry conditions reinforces the value of integrating climatic context into productivity assessments. Altogether, the interplay between land-cover change and productivity dynamics underscores that recent improvements stem partly from targeted restoration efforts, yet persistent deforestation, urban expansion and climatic variability continue to threaten the progress toward land-degradation neutrality.

4.2. Climate–Productivity Coupling and Indicator Reliability

The study area spans strong climatic gradients, ranging from humid Mediterranean conditions to arid desert environments, resulting in pronounced spatio-temporal variability in precipitation and temperature. Satellite-based analyses indicate that cropland area increased from 10% of total land in 2001 to 13.5% in 2010, before returning to approximately 10% by 2023 as barren land expanded and

 doi:10.20944/preprints202603.0221.v1

rainfall declined [47]. Over the same period, land surface temperature increased by up to 0.07 °C year^{-1}, while precipitation decreased by as much as 59 mm year^{-1} [47]. More than 60% of agricultural zones experienced declining NDVI and rainfall variability exceeding 100% in coefficient of variation [47]. These findings support the interpretation that vegetation dynamics in semi-arid environments are tightly coupled to rainfall variability.

The weak positive correlation between precipitation and NDVI, and the negative correlations observed for RUE and RESTREND (Table 5), illustrate the conceptual differences among productivity indicators. NDVI is directly sensitive to rainfall fluctuations and may therefore reflect short-term climatic variability rather than structural land-condition change. In contrast, RUE normalizes vegetation response by precipitation, and RESTREND statistically removes linear rainfall effects through regression analysis. These rainfall-adjusted metrics are designed to isolate residual vegetation trends that may be more closely associated with management practices or ecosystem resilience. However, each indicator captures different dimensions of productivity dynamics, and none can be considered universally superior without independent validation.

The hybrid productivity approach integrates NDVI, RUE, and RESTREND within a precipitation-conditioned framework. Specifically, RUE is applied under increasing precipitation conditions, NDVI under relatively stable rainfall, and RESTREND under declining precipitation regimes. Rather than asserting improved accuracy, this approach operationalizes the complementary strengths of existing indicators within a single, rule-based framework. The hybrid method therefore represents an alternative implementation of the land productivity sub-indicator that can be incorporated into land degradation (LD) assessments alongside established metrics. By explicitly accounting for precipitation trends, it provides a structured means of interpreting vegetation dynamics under varying climatic contexts and supports more nuanced analysis of productivity change across environmental gradients.

4.3. Anthropogenic Drivers of Land Degradation

Climatic variability explains much of the short-term fluctuation in land productivity; however, human activities remain dominant drivers of long-term land degradation in many dryland regions. Unsustainable agricultural practices, overgrazing and poor water management degrade soil structure and reduce vegetation cover. In arid and semi-arid environments, overgrazing driven by livestock demand strips vegetation and leaves soils exposed to wind and water erosion [48]. The loss of vegetation due to overgrazing or deforestation exposes soil surfaces to erosion processes and reduces primary productivity. Poor irrigation and drainage practices contribute to salinization, which impairs crop growth, damages soil structure and reduces long-term fertility [49]. The accumulation of salts in soil or water is frequently linked to inadequate land and water management.

Water scarcity further exacerbates degradation pressures across drylands. Long-term observations indicate declining precipitation trends and rising temperatures in many semi-arid regions, increasing evapotranspiration demand and reducing soil moisture availability. Renewable water resources have declined substantially in several countries over recent decades, pushing some areas close to absolute water-scarcity thresholds. Rain-fed agriculture often dominates cultivated land in drylands and supports a large share of rural livelihoods, while agriculture typically consumes the majority of mobilized freshwater resources. Deforestation, rangeland conversion and urban expansion also contribute to land degradation. Economic assessments consistently show that land degradation imposes substantial national costs through reduced agricultural and grazing productivity. These patterns underscore the need to address anthropogenic drivers through sustainable land management practices such as controlled grazing, conservation agriculture, soil organic matter enhancement and efficient irrigation. The hybrid productivity indicator presented here can support such efforts by identifying areas of declining, stable or improving productivity within the land productivity (LP) sub-indicator of SDG 15.3.1.

 doi:10.20944/preprints202603.0221.v1

4.4. Land Degradation Neutrality Commitments and Societal Relevance

Many countries have committed to achieving Land Degradation Neutrality (LDN) by 2030 under the UNCCD framework [50]. These commitments are typically supported by national sustainable development strategies and climate adaptation initiatives aimed at strengthening soil management, improving agricultural water control, enhancing climate risk management and mobilizing financing for restoration. Partnerships between public institutions, development banks and restoration funds are increasingly being used to rehabilitate degraded lands and restore ecosystem services.

The spatially explicit SDG 15.3.1 assessment developed in this study provides information that can inform national LDN roadmaps. By quantifying land degradation at 30 m resolution, priority zones for restoration and sustainable land management can be identified across croplands, rangelands and peri-urban areas. The hybrid productivity indicator offers an additional option for assessing the LP sub-indicator by integrating NDVI-, RUE- and RESTREND-based information within a precipitation-conditioned framework. Rather than relying on a single metric, this approach enables comparison among productivity indicators and supports climate-aware interpretation of trends. Binary land degradation maps derived using Rule B provide a conservative baseline against which progress toward LDN can be monitored. Linking spatial degradation patterns to socio-economic indicators such as poverty, food security and yield variability can further enhance policy relevance.

4.5. Uncertainties, Limitations and Misclassification Risk

Several sources of uncertainty may influence the magnitude, though not necessarily the spatial patterns, of land degradation reported here. First, satellite-derived precipitation datasets may contain biases in arid regions with sparse gauge networks, which can influence RUE and RESTREND calculations. Second, the use of IPCC Tier 1 soil organic carbon (SOC) coefficients assumes homogeneous soil properties and management practices; this may over- or under-estimate carbon changes for specific land-use transitions. Third, Landsat 7 ETM+ data are affected by scan-line failure; although gap-filling procedures were applied, residual artefacts may persist. Fourth, the absence of national-scale field validation means that classifications rely exclusively on remote sensing products. In situ measurements of vegetation productivity and SOC would enable formal accuracy assessment. Fifth, the three-class scheme (declining, stable, improving) and the $\pm 10\%$ SOC threshold recommended by the GPG simplify a continuum of change and may mask subtle but ecologically relevant trends. Finally, Rule B for binary land degradation mapping intentionally flags areas that are worsening even if not yet fully degraded; this precautionary approach supports early warning but may overestimate irreversible degradation. Future research should incorporate higher-resolution precipitation datasets, soil-adjusted vegetation indices (e.g., MSAVI2 or SAVI), and field observations to refine LP estimates and improve validation.

4.6. Scaling, Transferability and Future Research

The methodology presented here is transferable to other dryland contexts due to its reliance on openly available satellite datasets and cloud-based processing platforms. The hybrid productivity framework can be adapted to different climatic regimes by adjusting precipitation thresholds or decision rules used to select among NDVI, RUE and RESTREND metrics. Additional climatic drivers such as temperature anomalies, evapotranspiration and soil moisture could be incorporated to further refine the decision logic. Improved SOC datasets from national soil surveys or emerging high-resolution soil mapping initiatives would enhance the accuracy of the SOC sub-indicator. Field campaigns designed to validate land-cover transitions, productivity estimates and SOC changes would strengthen confidence in remote-sensing-based SDG 15.3.1 assessments.

Beyond individual case studies, the precipitation-conditioned hybrid indicator provides an alternative approach for evaluating the LP component of SDG 15.3.1 in climate-sensitive environments. Cloud-computing platforms enable rapid scaling across countries without extensive local computational resources. Integrating land-degradation assessments with socio-economic indicators and

 doi:10.20944/preprints202603.0221.v1

participatory approaches such as farmer surveys or citizen science initiatives could improve interpretation and support locally appropriate restoration strategies.

5. Conclusions

This study presents a climate-aware assessment framework for land degradation using high-resolution remote sensing and a precipitation-conditioned hybrid land productivity indicator. By integrating land-cover transitions, soil organic carbon changes and multiple productivity metrics, a spatially explicit SDG 15.3.1 indicator was derived that enables comparison among NDVI-, RUE- and RESTREND-based LP assessments. Results demonstrate that productivity trends are highly sensitive to climatic variability: NDVI alone may reflect rainfall fluctuations, whereas RUE and RESTREND adjust for precipitation effects in different ways. The hybrid framework offers an additional option for implementing the LP sub-indicator by selecting among these metrics according to precipitation conditions, thereby supporting climate-aware interpretation of land productivity dynamics.

Anthropogenic pressures including overgrazing, unsustainable agriculture, water mismanagement and land-use change remain key contributors to long-term degradation in drylands. Achieving Land Degradation Neutrality will require targeted investments, improved monitoring systems and stakeholder engagement. The hybrid methodology developed here relies exclusively on open datasets and cloud-based tools, making it adaptable to other dryland regions. Its application can support more context-sensitive SDG 15.3.1 reporting and inform sustainable land management and restoration planning.

Author Contributions: Conceptualization, N.R., N.A. and O.D; methodology, N.R., N.A and O.D; software, N.R.; validation, N.R., N.A. and O.D.; formal analysis, N.R., N.A. and O.D.; investigation, N.R.and N.A. ; data curation, N.R.and N.A.; writing—original draft preparation, N.R.; writing—review and editing, N.R. and N.A. ; visualization, N.R.and N.A.; supervision, O.D.; project administration, O.D.; funding acquisition, O.D. All authors have read and agreed to the published version of the manuscript.

Funding: This project has received funding from the European Union's Horizon Europe research and innovation programme under Grant Agreement No. 101086250 – EWALD.

Data Availability Statement: The data presented in this study are available on request from the corresponding author. The data are not publicly available due to the large amount of data.

Conflicts of Interest: The authors declare no conflicts of interest.

List of Abbreviations

Land Degradation and Productivity Indicators

LC Land Cover; one of the three sub-indicators of the SDG 15.3.1 framework

LCC Land Cover Change

LD Land Degradation; reduction or loss of biological or economic productivity

LP Land Productivity; capacity of vegetation to convert resources into biomass

NDVI Normalized Difference Vegetation Index

NDWI Normalized Difference Water Index

NPP Net Primary Productivity

RESTREND Residual Trends; method to isolate climate-independent vegetation changes

RUE Rain Use Efficiency; vegetation productivity normalized by precipitation

SOC Soil Organic Carbon

MSAVI2 Modified Soil Adjusted Vegetation Index 2

SAVI Soil Adjusted Vegetation Index

 doi:10.20944/preprints202603.0221.v1

Frameworks, Organizations, and Policies

LDN Land Degradation Neutrality

SDG Sustainable Development Goal (Indicator 15.3.1)

UNCCD United Nations Convention to Combat Desertification

IPCC Intergovernmental Panel on Climate Change

AAA Adaptation of African Agriculture

NSSD National Strategy for Sustainable Development (Morocco NSSD 2030)

UNEP United Nations Environment Programme

CBD Convention on Biological Diversity

Datasets, Platforms, and Technical Terms

CHIRPS Climate Hazards Group InfraRed Precipitation with Stations

GEE Google Earth Engine

GPG Good Practice Guidance (UNCCD)

GLC_FCS30D Global Land Cover Dataset with Fine Classification System (30 m)

MODIS Moderate Resolution Imaging Spectroradiometer

AVHRR Advanced Very High Resolution Radiometer

ETM+ Enhanced Thematic Mapper Plus (Landsat 7)

iSDA Innovative Solutions for Decision Agriculture

OLS Ordinary Least Squares

P Precipitation

AFOLU Agriculture, Forestry and Other Land Use

Units and Miscellaneous

Mha Million hectares

ha Hectares

GDP Gross Domestic Product

USD United States Dollar

COP Conference of the Parties

r Pearson correlation coefficient

Z Standardized Z-score

 doi:10.20944/preprints202603.0221.v1

Appendix A. Land Cover Transition Matrix

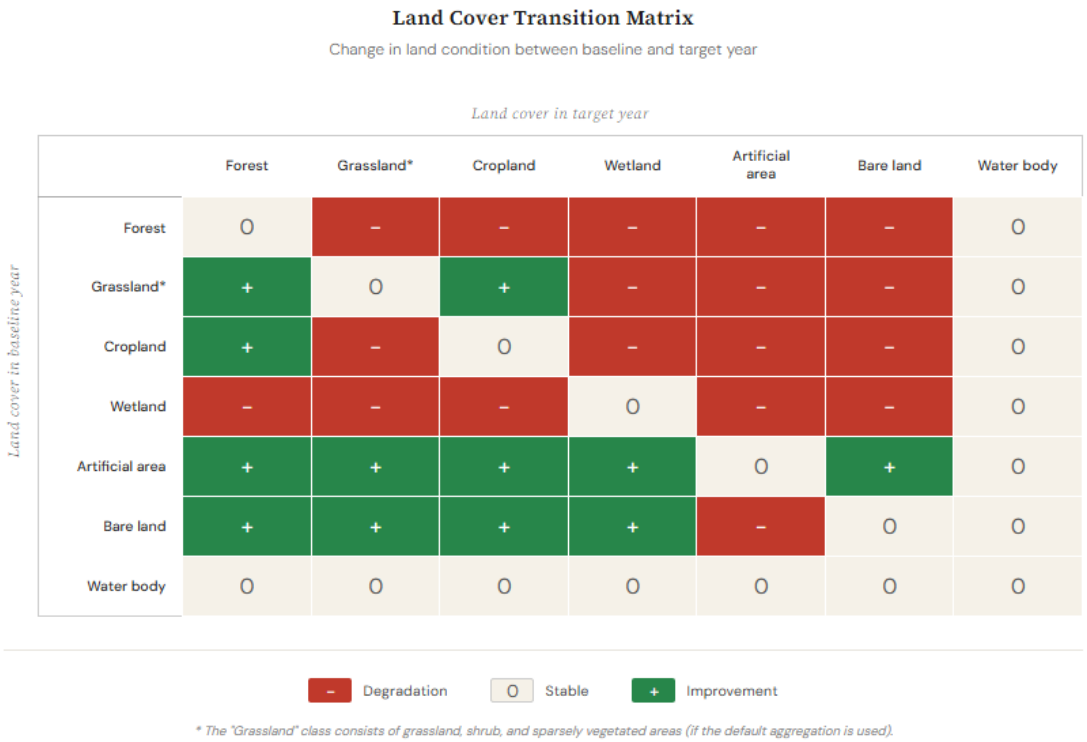

Land cover in baseline year \ Land cover in target year	Forest	Grassland*	Cropland	Wetland	Artificial area	Bare land	Water body
Forest	0	–	–	–	–	–	0
Grassland*	+	0	+	–	–	–	0
Cropland	+	–	0	–	–	–	0
Wetland	–	–	–	0	–	–	0
Artificial area	+	+	+	+	0	+	0
Bare land	+	+	+	+	–	0	0
Water body	0	0	0	0	0	0	0

Figure A1. Land Cover Transition Matrix between baseline and target year.

 doi:10.20944/preprints202603.0221.v1

Appendix B. Land Productivity Decision Table Based on GPG version 2

Land Productivity Decision Table (Color-Coded by GPG Version 2)

Trend	State	Performance	GPG Version 2
Degraded	Degraded	Degraded	Degraded
Degraded	Degraded	Not degraded	Degraded
Degraded	Stable	Degraded	Degraded
Degraded	Stable	Not degraded	Stable
Degraded	Improved	Degraded	Degraded
Degraded	Improved	Not degraded	Stable
Stable	Degraded	Degraded	Degraded
Stable	Degraded	Not degraded	Stable
Stable	Stable	Degraded	Stable
Stable	Stable	Not degraded	Stable
Stable	Improved	Degraded	Stable
Stable	Improved	Not degraded	Stable
Improved	Degraded	Degraded	Degraded
Improved	Degraded	Not degraded	Improved
Improved	Stable	Degraded	Improved
Improved	Stable	Not degraded	Improved
Improved	Improved	Degraded	Improved
Improved	Improved	Not degraded	Improved

Figure B1. Land Productivity Decision Table based on GPG version 2

Appendix C. Logic of Rule B

Rule B generates a binary land degradation map by identifying pixels that are either currently degraded or have worsened relative to the baseline period. This approach aligns with the SDG 15.3.1 methodology, which classifies land as degraded if it is presently in a degraded state *or* has experienced a decline in condition over time.

Definition

Let $B(x)$ and $M(x)$ denote the baseline and monitoring classifications for pixel x, where the three ordinal classes are:

Value	Class
1	Degraded (worst)
2	Stable
3	Improving (best)

Two intermediate indicators are defined as follows:

 doi:10.20944/preprints202603.0221.v1

$$\text{DegradedNow}(x) = \begin{cases} 1 & \text{if } M(x) = 1 \\ 0 & \text{otherwise} \end{cases} \qquad \text{Worsened}(x) = \begin{cases} 1 & \text{if } M(x) < B(x) \\ 0 & \text{otherwise} \end{cases}$$

The final binary degradation status is then computed as:

$$\text{BinaryLD}(x) \;=\; \text{DegradedNow}(x) \vee \text{Worsened}(x)$$

where $\text{BinaryLD}(x) = 1$ indicates a **degraded** pixel and $\text{BinaryLD}(x) = 0$ indicates a **non-degraded** pixel.

Illustrative Example

Table C1 walks through representative combinations of baseline and monitoring values to illustrate how Rule B operates in practice.

Table C1. Illustration of Rule B for converting three-class SDG 15.3.1 maps to a binary land degradation layer. Rows above the mid-rule are classified as degraded (BinaryLD = 1); rows below are non-degraded (BinaryLD = 0).

Baseline $B(x)$	**Monitoring** $M(x)$	**DegradedNow**	**Worsened**	**BinaryLD**
3	2	0	1	**1**
3	1	1	1	**1**
2	1	1	1	**1**
1	2	0	0	0
1	3	0	0	0
2	2	0	0	0

A pixel is classified as degraded if it is currently in the degraded class ($M(x) = 1$) *or* if its condition has worsened relative to the baseline ($M(x) < B(x)$), regardless of its absolute monitoring value.

Appendix D. Land Cover Transition Matrices

From 2000 to 2015

Table D1. Land cover transitions from 2000 (baseline) to 2015 (monitoring), in Mha.

From (2000) \To (2015)	Forest	Grassland	Cropland	Wetland	Artificial	Other	Water
Forest	9.84	0.17	0.00	0.00	0.06	0.83	0.00
Grassland	0.13	1.43	0.00	0.00	0.00	0.08	0.00
Cropland	0.00	0.00	0.00	0.00	0.00	0.00	0.00
Wetland	0.00	0.00	0.00	0.02	0.00	0.00	0.01
Artificial	0.02	0.00	0.00	0.00	0.21	0.03	0.00
Other Land	1.08	0.13	0.00	0.01	0.05	29.02	0.00
Water Body	0.00	0.00	0.00	0.00	0.00	0.00	0.04

 doi:10.20944/preprints202603.0221.v1

From 2015 to 2022

Table D2. Land cover transitions from 2015 (baseline) to 2022 (monitoring), in Mha.

From (2015) \To (2022)	Forest	Grassland	Cropland	Wetland	Artificial	Other	Water
Forest	10.07	0.10	0.00	0.00	0.02	0.87	0.00
Grassland	0.11	1.54	0.00	0.00	0.00	0.08	0.00
Cropland	0.00	0.00	0.00	0.00	0.00	0.00	0.00
Wetland	0.01	0.00	0.00	0.02	0.00	0.01	0.00
Artificial	0.02	0.00	0.00	0.00	0.27	0.02	0.00
Other Land	0.60	0.07	0.00	0.00	0.03	29.26	0.00
Water Body	0.00	0.00	0.00	0.01	0.00	0.01	0.04

Appendix E. Cross-Comparison of Precipitation and LP Trends

Monitoring Period

Table E1. Cross-comparison of precipitation and LP trends during the monitoring period. Each value represents the percentage of area falling under Declining, Stable, and Improving land productivity categories under different precipitation trends.

Precipitation Trend	**LP Category**	**NDVI (%)**	**RUE (%)**	**RESTREND (%)**
Decreasing	Declining	2.92	0.02	0.02
	Stable	7.22	4.70	5.35
	Improving	0.57	5.99	5.33
Stable	Declining	10.38	0.35	0.32
	Stable	71.93	84.96	84.77
	Improving	5.42	2.40	2.62
Increasing	Declining	0.02	0.09	0.08
	Stable	1.29	1.47	1.47
	Improving	0.25	0.00	0.00

 doi:10.20944/preprints202603.0221.v1

Baseline Period

Table E2. Cross-comparison of precipitation and LP trends during the baseline period. Each value represents the percentage of area falling under Declining, Stable, and Improving land productivity categories under different precipitation trends.

Precipitation Trend	LP Category	NDVI (%)	RUE (%)	RESTREND (%)
Decreasing	Declining	0.00	0.00	0.00
	Stable	0.02	0.03	0.02
	Improving	0.42	0.42	0.42
Stable	Declining	0.07	0.07	0.10
	Stable	35.79	4.50	35.86
	Improving	24.54	55.84	24.44
Increasing	Declining	0.26	0.01	0.28
	Stable	37.04	0.70	36.86
	Improving	1.84	38.42	1.99

References

1. UNCCD. Elaboration of an International Convention to Combat Desertification..., 1994. Available online: https://catalogue.unccd.int/936_UNCCD_Convention_ENG.pdf (accessed 1 February 2026).
2. UNCCD. Global Land Outlook: First Edition, 2017. Available online: https://www.unccd.int/sites/default/files/documents/2017-09/GLO_Full_Report_low_res.pdf (accessed 1 February 2026).
3. Prăvălie, R.; et al. A Unifying Modelling of Multiple Land Degradation Pathways in Europe. *Nature Communications* **2024**, *15*, 3862. https://doi.org/10.1038/s41467-024-48252-x.
4. UNCCD. Global Land Outlook: Second Edition, 2022. Available online: https://www.unccd.int/sites/default/files/2022-04/UNCCD_GLO2_low-res_2.pdf (accessed 1 February 2026).
5. Boughlala, M.; Dahan, R.; Mrabet, R.; Laamari, A.; Balaghi, R.; Lajouad, L. A Review of Available Knowledge on Land Degradation in Morocco, 2013. Available online: https://ageconsearch.umn.edu/record/253831/files/OASIS_2_Morocco%20_1_.pdf (accessed 1 February 2026).
6. UNCCD. Achieving Land Degradation Neutrality, 2016. Available online: https://www.unccd.int/sites/default/files/documents/18102016_LDN%20country%20level_ENG.pdf (accessed 1 February 2026).
7. D'Acunto, F.; Marinello, F.; Pezzuolo, A. Rural Land Degradation Assessment through Remote Sensing: Current Technologies, Models, and Applications. *Remote Sensing* **2024**, *16*, 3059. https://doi.org/10.3390/rs16163059.
8. Dubovyk, O. The Role of Remote Sensing in Land Degradation Assessments: Opportunities and Challenges. *European Journal of Remote Sensing* **2017**, *50*, 601–613. https://doi.org/10.1080/22797254.2017.1378926.
9. Kimura, R.; Moriyama, M. Determination by MODIS satellite-based methods of recent global trends in land surface aridity and degradation. *Journal of Agricultural Meteorology* **2019**, *75*, 153–159. https://doi.org/10.2480/agrmet.D-19-00003.
10. Conservation International. Trends.Earth User Guide, Version 2.17, 2025. Available online: https://docs.trends.earth/en/latest/for_users/index.html (accessed 1 February 2026).
11. Kirui, O.K.; Mirzabaev, A.; von Braun, J. Assessment of land degradation 'on the ground' and from 'above'. *SN Applied Sciences* **2021**, *3*, 318. https://doi.org/10.1007/s42452-021-04314-z.
12. Adesina, E.A.; Muhammad, H.I. Assessment of land degradation using remote sensing approach. *Geodesy and Cartography* **2023**, *49*, 142–148. https://doi.org/10.3846/gac.2023.16007.
13. UNCCD. Good Practice Guidance for SDG Indicator 15.3.1, Version 1.0, 2017. Available online: https://catalogue.unccd.int/1531_Good_Practice_Guidance_SDG_Indicator_15.3.1_Version_1.0.pdf (accessed 1 February 2026).
14. Reith, J.; Ghazaryan, G.; Muthoni, F.; Dubovyk, O. Assessment of Land Degradation in Semiarid Tanzania–Using Multiscale Remote Sensing Datasets to Support Sustainable Development Goal 15.3. *Remote Sens.* **2021**, *13*, 1754. https://doi.org/10.3390/rs13091754.

 doi:10.20944/preprints202603.0221.v1

15. UNCCD. Good Practice Guidance for SDG Indicator 15.3.1, Version 2.0, 2023. Available online: https://www.unccd.int/sites/default/files/documents/2021-09/UNCCD_GPG_SDG-Indicator-15.3.1_version2_2021.pdf (accessed 1 February 2026).
16. Lamaamri, M.; Lghabi, N.; Ghazi, A.; et al. Evaluation of Desertification in the Middle Moulouya Basin (North-East Morocco) Using Sentinel-2 Images and Spectral Index Techniques. *Earth Systems and Environment* **2023**, *7*, 473–492. https://doi.org/10.1007/s41748-022-00327-9.
17. Ramírez-Juidias, E.; et al. Applying Remote Sensing Methods to Estimate Alterations in Land Cover Change and Degradation in the Desert Regions of the Southeast Iberian Peninsula. *Remote Sensing* **2023**, *15*, 3984. https://doi.org/10.3390/rs15163984.
18. Evans, J.; Geerken, R. Discrimination between climate and human-induced dryland degradation. *Journal of Arid Environments* **2004**, *57*, 535–554. https://doi.org/10.1016/S0140-1963(03)00121-6.
19. Wessels, K.J.; Prince, S.D.; Frost, P.E.; van Zyl, D. Assessing the effects of human-induced land degradation in the former homelands of northern South Africa with a 1 km AVHRR NDVI time-series. *Remote Sensing of Environment* **2004**, *91*, 47–67. https://doi.org/10.1016/j.rse.2004.02.005.
20. Bai, Z.G.; Dent, D.L.; Olsson, L.; Schaepman, M.E. Proxy global assessment of land degradation. *Soil Use and Management* **2008**, *24*, 223–234. https://doi.org/10.1111/j.1475-2743.2008.00169.x.
21. Burrell, A.L.; Evans, J.P.; Liu, Y. Detecting dryland degradation using Time Series Segmentation and Residual Trend analysis (TSS-RESTREND). *Remote Sensing of Environment* **2017**, *197*, 43–57. https://doi.org/10.1016/j.rse.2017.05.018.
22. Le Houérou, H.N. Rain use efficiency: a unifying concept in arid-land ecology. *Journal of Arid Environments* **1984**, *7*, 213–247. https://doi.org/10.1016/S0140-1963(18)31362-4.
23. Wessels, K.J.; van den Bergh, F.; Scholes, R.J. Limits to detectability of land degradation by trend analysis of vegetation index data. *Remote Sensing of Environment* **2012**, *125*, 10–22. https://doi.org/10.1016/j.rse.2012.06.022.
24. Moussa, S.; El Brirchi, E.H.; Alami, O.B. Monitoring Land Productivity Trends in Souss-Massa Region Using Landsat Time Series Data to Support SDG Target 15.3. In *Geospatial Intelligence*; Springer, 2022; pp. 109–121. https://doi.org/10.1007/978-3-030-80458-9_9.
25. Laamouri, A.; Khattabi, A. Estimating the Economic Cost of Land Degradation and Desertification in Morocco. *Land* **2025**, *14*, 837. https://doi.org/10.3390/land14040837.
26. El Mrini, A.; Anthony, E.J.; Maanan, M.; Taaouati, M.; Nachite, D. Beach-dune degradation in a Mediterranean context of strong development pressures, and the missing integrated management perspective. *Ocean & Coastal Management* **2012**, *69*, 299–306. https://doi.org/10.1016/j.ocecoaman.2012.08.004.
27. Laamouri, A.; Khattabi, A. Estimating the Economic Cost of Land Degradation and Desertification in Morocco. *Land* **2025**, *14*, 837. https://doi.org/10.3390/land14040837.
28. Zhang, X.; Liu, L.; Chen, X.; Xie, S.; Gao, Y. A Global 30 m Land-Cover Dataset with Fine Classification System (GLC_FCS30D) for 2000–2020. *Science Bulletin* **2021**, *66*, 1817–1825. https://doi.org/10.1016/j.scib.2021.08.003.
29. Wulder, M.A.; Loveland, T.R.; Roy, D.P.; Crawford, C.J.; Masek, J.G. Current Status of the Landsat Program, Science, and Applications. *Remote Sensing of Environment* **2019**, *225*, 127–147. https://doi.org/10.1016/j.rse.2019.02.015.
30. Funk, C.; Peterson, P.; Landsfeld, M.; Pedreros, D.; Verdin, J. The Climate Hazards Infrared Precipitation with Stations—A New Environmental Record for Monitoring Extremes. *Scientific Data* **2015**, *2*, 150066. https://doi.org/10.1038/sdata.2015.66.
31. Hengl, T.; de Jesus, J.M.; Heuvelink, G.B.M.; Gonzalez, M.R.; Kilibarda, M. SoilGrids250m: Global Gridded Soil Information Based on Machine Learning. *PLOS ONE* **2017**, *12*, e0169748. https://doi.org/10.1371/journal.pone.0169748.
32. Sims, N.C.; Green, C.; Newnham, G.; England, J.; Held, A. Developing Good Practice Guidance for Estimating Land Degradation in the Context of the United Nations Sustainable Development Goals. *Environmental Science & Policy* **2019**, *92*, 349–355. https://doi.org/10.1016/j.envsci.2018.10.014.
33. Duarte-Guardia, S.; Peri, P.L.; Calandroni, M.; Rubio, G. Soils Need to Be Considered When Assessing the Impacts of Land-Use Change on Carbon Sequestration. *Nature Ecology & Evolution* **2019**, *3*, 1642. https://doi.org/10.1038/s41559-019-1026-8.
34. IPCC. 2006 IPCC Guidelines for National Greenhouse Gas Inventories. Volume 4: Agriculture, Forestry and Other Land Use (AFOLU), 2006. Available online: https://www.ipcc-nggip.iges.or.jp/public/2006gl/vol4.html (accessed 1 February 2026).

 doi:10.20944/preprints202603.0221.v1

35. Zhao, M.; Running, S.W. Drought-Induced Reduction in Global Terrestrial Net Primary Production from 2000 through 2009. *Science* **2010**, *329*, 940–943. https://doi.org/10.1126/science.1192666.
36. Pettorelli, N.; Vik, J.O.; Mysterud, A.; Gaillard, J.M.; Tucker, C.J.; Stenseth, N.C. Using the Satellite-Derived NDVI to Assess Ecological Responses to Environmental Change. *Trends in Ecology & Evolution* **2005**, *20*, 503–510. https://doi.org/10.1016/j.tree.2005.05.011.
37. Ivits, E.; Cherlet, M.; Mehl, W.; Sommer, S. Addressing the Complexity in Non-Linear Evolution of Vegetation Phenological Change with Remote Sensing. *Ecological Indicators* **2012**, *26*, 49–60. https://doi.org/10.1016/j.ecolind.2012.10.007.
38. Le, Q.B.; Nkonya, E.; Mirzabaev, A. Biomass Productivity-Based Mapping of Global Land Degradation Hotspots. In *Economics of Land Degradation and Improvement – A Global Assessment for Sustainable Development*; Nkonya, E.; Mirzabaev, A.; von Braun, J., Eds.; Springer: Cham, 2016. https://doi.org/10.1007/978-3-319-19168-3_4.
39. Mann, H.B. Nonparametric tests against trend. *Econometrica: Journal of the econometric society* **1945**, pp. 245–259. https://doi.org/https://doi.org/10.2307/1907187.
40. Kendall, M.G. Rank correlation methods. **1948**.
41. Wessels, K.J.; Prince, S.D.; Malherbe, J.; Small, J. Can Human-Induced Land Degradation Be Distinguished from the Effects of Rainfall Variability? A Case Study in South Africa. *Journal of Arid Environments* **2007**, *68*, 271–297. https://doi.org/10.1016/j.jaridenv.2006.05.015.
42. Cowie, A.L.; Orr, B.J.; Sanchez, V.M.C.; Chasek, P.; Crossman, N.D.; Erlewein, A.; Louwagie, G.; Maron, M.; Metternicht, G.I.; Minelli, S.; et al. Land in balance: The scientific conceptual framework for Land Degradation Neutrality. *Environmental science & policy* **2018**, *79*, 25–35. https://doi.org/10.1016/j.envsci.2017.10.011.
43. Roy, D.P.; Kovalskyy, V.; Zhang, H.; Vermote, E.F.; Yan, L.; Kumar, S.; Egorov, A. Characterization of Landsat-7 to Landsat-8 reflective wavelength and normalized difference vegetation index continuity. *Remote sensing of Environment* **2016**, *185*, 57–70. https://doi.org/10.1016/j.rse.2015.12.024.
44. Convention on Biological Diversity (CBD). Country Profile – Morocco. Technical report, CBD Secretariat, Montreal, Canada, 2022.
45. Li, L.; Xia, R.; Dou, M.; Ling, M.; Li, G.; Wang, C.; Mi, Q. Integrating Landsat NDVI data with climate and anthropogenic factors reveals drivers of vegetation dynamics in the semi-arid Basin of Western China. *Scientific Reports* **2025**, *15*, 18831. https://doi.org/10.1038/s41598-025-02360-w.
46. Sharma, M.; Bangotra, P.; Gautam, A.S.; et al. Sensitivity of normalized difference vegetation index (NDVI) to land surface temperature, soil moisture and precipitation over district Gautam Buddh Nagar, UP, India. *Stochastic Environmental Research and Risk Assessment* **2022**, *36*, 1779–1789. https://doi.org/10.1007/s00477-021-02066-1.
47. Alvarez, C.I.; Govind, A. Assessing climate and land use changes in Morocco (2001–2023): from a geospatial and farmers' perspective. *Theoretical and Applied Climatology* **2025**, *156*, 420. https://doi.org/10.1007/s00704-025-05656-z.
48. Klik, A.; Kaitna, R.; Badraoui, M. Desertification hazard in a mountainous ecosystem in the High Atlas region, Morocco. In Proceedings of the Proceedings of the 12th International Soil Conservation Organization Conference, Beijing, China, 2002. Available online: https://topsoil.nserl.purdue.edu/isco/isco12/VolumeIV/DesertificationHazard.pdf (accessed 1 February 2026).
49. The Salt Doctors and Acacia Water. Saline Farming Assessment Mission – Morocco, 2022. Available online: https://www.rvo.nl/sites/default/files/2024-01/saline-farming-assessment-mission-morocco.pdf (accessed 1 February 2026).
50. UNCCD. Land Degradation Neutrality (LDN), 2024.